



# Improved direct inverse tracking control of a piezoelectric tube scanner for high-speed AFM imaging<sup>☆</sup>



Han Lu, Yongchun Fang<sup>\*</sup>, Xiao Ren, Xuebo Zhang

*Institute of Robotics and Automatic Information System, Nankai University, Tianjin 300071, PR China  
Tianjin Key Laboratory of Intelligent Robotics, Tianjin 300071, PR China*

## ARTICLE INFO

### Article history:

Received 31 January 2015  
Revised 24 June 2015  
Accepted 19 August 2015  
Available online 1 October 2015

### Keywords:

Piezoelectric tube scanner (PTS)  
Atomic force microscope (AFM)  
Prandtl–Ishlinskii (P–I)  
Tracking control  
Feedforward control

## ABSTRACT

For a piezoelectric tube scanner (PTS), this paper proposes an improved direct inverse tracking control algorithm and apply it to an atomic force microscope (AFM) to accomplish high-speed scanning tasks. That is, to enhance the high-speed tracking control performance of a PTS, an improved direct inverse rate-dependent Prandtl–Ishlinskii (P–I) model is firstly constructed, which includes a polynomial module to eliminate the structure nonlinearity. Based on the model, a practical feedforward control law is then designed to implement high-speed tracking control for a high-frequency trajectory with strong robustness, which presents the advantages of high-speed response, simple structure and convenient implementation. Subsequently, the designed feedforward law is combined with a feedback component, and the combined control strategy is employed in an AFM to accomplish fast imaging tasks. Numerous experimental results are then collected, which convincingly demonstrate the superior performance of the proposed practical model/control scheme.

© 2015 Elsevier Ltd. All rights reserved.

## 1. Introduction

Piezoelectric actuators are playing an important role in nanotechnology due to their good performance [1–5] in micro/nano scale positioning and signal tracking. Different from certain integrated piezo-flexural mechanisms [6], a piezoelectric tube scanner (PTS) provides 3 degrees of freedom (DOF) displacements and presents such obvious advantages as low cost, simple structure, convenience for function extension, and so on.

Commonly employed in an atomic force microscope (AFM) [7] as a scanner, a PTS contributes a lot in micro/nano scale imaging and manipulations [8–12]. An AFM in contact constant-force mode works in the following way (see Fig. 1): first, a bendable cantilever with a rigid probe is placed above the sample surface; then a PTS is actuated by two scanning signals to move in horizontal direction, simultaneously actuated in the vertical direction to keep relative displacement between the tip of the probe and the sample as a constant; with the sample surface ‘disturbance’ signal recorded by a laser launch/detection system, and together with all the scanning signals, a complete vivid micro/nano scale surface image is

finally obtained. Considering the requirement of high-speed, high precision AFM scanning, it is highly required to design practical control laws, which enable a PTS to track high-frequency trajectories, so as to implement fast imaging tasks. Unfortunately, the non-linear behavior of a PTS, such as hysteresis, creep, vibrations, modeling error and rate-dependent behavior, largely reduces its positioning performance [8], and then makes its control a very challenging problem [9].

When designing control strategies for a PTS, feedback control is always the first choice, where a linearized model is usually identified through experimental data, based on which, distinct feedback approaches can be adopted to construct proper controllers. For examples, Das et al. apply a double resonant controller in [10] to damp out the first resonant mode of the PTS and increase the closed-loop bandwidth; an optimal linear quadratic Gaussian (LQG) controller with a vibration compensator is designed by Habibullah et al. in [11] for the same purpose; Rana et al. employ an improved model predictive control (MPC) scheme in [12] to achieve high-speed scanning performance. Although good tracking accuracy may be achieved by a well-designed feedback controller alone, a phase-lag between the control input and the plant response usually exists. Besides, large sensor noises or modeling error can possibly lead to unacceptable tracking error or even system instability, especially when tracking trajectories with sufficiently high frequencies.

<sup>☆</sup> Supported by National Natural Science Foundation (NNSF) of China (61127006).

<sup>\*</sup> Corresponding author at: Institute of Robotics and Automatic Information System, Nankai University, Tianjin 300071, PR China.

E-mail addresses: [luhan@mail.nankai.edu.cn](mailto:luhan@mail.nankai.edu.cn) (H. Lu), [fangyc@nankai.edu.cn](mailto:fangyc@nankai.edu.cn) (Y. Fang), [renx@mail.nankai.edu.cn](mailto:renx@mail.nankai.edu.cn) (X. Ren), [zhangxuebo@nankai.edu.cn](mailto:zhangxuebo@nankai.edu.cn) (X. Zhang).

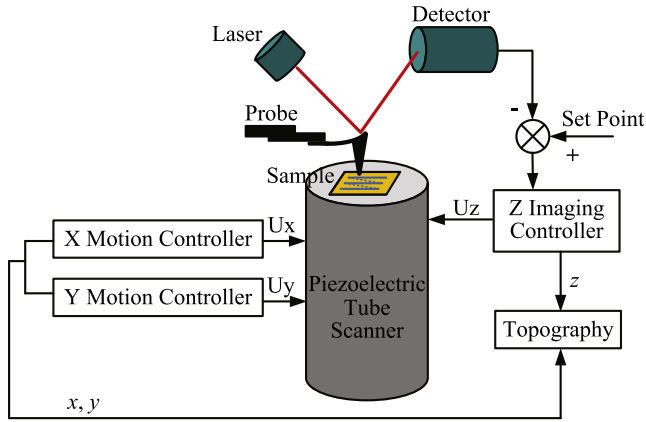


Fig. 1. Schematic of an AFM system.

Compared with feedback control, a feedforward controller is promising to provide a simpler and more effective way for high-frequency trajectory tracking control problem. Recently, the modeling and feedforward control problem for a PTS has received considerable interest. Prandtl–Ishlinskii (P–I) model [13–15] is one of the most widely used hysteresis models for nonlinearity compensation. Its inversion can be analytically calculated and it is also of P–I form [6,16]. Ang et al. in [16] propose a rate-dependent modified P–I operator to compensate the hysteresis nonlinearity at varying driving frequency. Qin et al. propose a direct inverse rate-dependent modeling approach, which can be directly derived from experimental data [6], so as to avoid complex inversion calculations. Recently, researchers try to combine various feedforward algorithms with feedback control law to achieve satisfactory control performance [17]. For examples, Leang et al. improve the tracking and positioning performance by adding a repetitive controller to the inverse feedforward hysteresis compensator in [18], and in [19], Leang and Devasia integrate the high-gain feedback-controller with a feedforward component to compensate the system vibration.

Inspired by the recent results of hybrid feedforward/feedback control structure [20], this paper proposes a practical feedback and feedforward combined control strategy for a PTS to eliminate/reduce the effects of nonlinear hysteresis and external disturbance, and then apply it to an AFM to accomplish high-speed imaging tasks. Specifically, we first introduce a polynomial module into the direct inverse P–I model to set up an improved rate-dependent model, which describes the characteristics of the PTS successfully. After identifying the system parameters, a compact feedforward control law is then constructed and combined with a standard feedback control law to form a practical control scheme with satisfactory performance. Subsequently, the control strategy is utilized on the AFM system, which, together with the spiral scanning pattern [21,22], successfully accomplishes high-speed imaging mode. Finally, some experimental results are collected to analyze the performance of the proposed control strategy. The contribution of the paper lies in the following aspects: i. a straightforward, yet accurate model is set up to describe the rate-dependent dynamics of the system, where a polynomial module is firstly introduced into the existing P–I model to provide better description of the system characteristics, whose accuracy is supported by experimental analysis; ii. a practical feedforward control strategy is proposed for the PTS, which presents the advantages of simple structure, easy implementation, and satisfactory performance; iii. the recently developed spiral scanning pattern is adopted into the AFM imaging system for high-speed scanning tasks.

The remainder of this paper is organized as follows. Section 2 introduces an improved direct inverse rate-dependent P–I model.

Section 3 describes the design of a compact feedforward control law and the overall control strategy in details. Section 4 provides sufficient experimental results and analysis to demonstrate the performance. Section 5 draws the conclusions.

## 2. Improved inverse rate-dependent model

As mentioned above, the nonlinear behavior of a piezoelectric tube scanner is quite complex, including hysteresis, creep, rate-dependent behavior, structural vibration, and so on [8]. As generally known, a P–I model is one of the most widely adopted pure phenomenological models which successfully describes the complex nonlinear behavior of a piezoelectric actuator. Therefore, in this research, we utilize P–I model to depict the behavior of the studied PTS.

### 2.1. Direct inverse rate-dependent P–I model

Considering the mathematical formulation, the direct inverse P–I model can be derived and expressed as follows [6,16]:

$$\hat{u}(t) = \mathbf{w}_h^T \cdot \mathbf{H}_r[S(y)](t) = \sum_{i=1}^n w_{hi} H_{ri}[S(y)](t) \quad (1)$$

where  $y(t)$  is the output of the PTS,  $\hat{u}(t)$  is the modeled control input of the PTS relative to the actual control input  $u(t)$ ,  $n$  is the number of thresholds, and  $\mathbf{r} = [r_1, r_2, \dots, r_n]^T$  is the threshold vector where we adopt the thresholds in the form of  $r_i = (i-1)/\max\{|y(t)|\}$ ,  $i = 0, 1, \dots, n$ .

In addition,  $\mathbf{H}_r[\cdot](t) = [H_{r1}[\cdot](t), H_{r2}[\cdot](t), \dots, H_{rn}[\cdot](t)]^T$  represents the elementary backlash operator vector, and  $\mathbf{w}_h = [w_{h1}, w_{h2}, \dots, w_{hn}]^T$  is the weight vector [6]. As can be seen from (1), the direct inverse P–I model is essentially the linear superposition of all the elementary backlash operators with different thresholds and weight values. Moreover,  $S(y)$  represents the saturation operator aiming at reshaping the hysteresis loop, which can be regarded as taking the form of multiple one-sided dead zone operators, or a polynomial formulation adopted in [6] as follows:

$$S(y) = c_m y^m + c_{m-1} y^{m-1} + \dots + c_1 y \quad (2)$$

with the vector form denoted as  $\mathbf{c} = [c_1, c_2, \dots, c_m]^T$ . Yet, it should be noted that this model is still rate-independent, which brings much difficulty for practical applications.

Considering inputs of different frequency, the work of Ang et al. and Tan et al. can be brought into model (1) to make it valid for a wide range of frequencies. As shown in [6,16], the rate-dependent behavior can be described in the way that the weights vary linearly against the control input rate while keeping other components unchanged. Based on this fact, (1) is rewritten into the direct inverse rate-dependent P–I model [6]:

$$\hat{u}(t) = (\mathbf{k}\dot{y}(t) + \mathbf{b})^T \cdot \mathbf{H}_r[S(y)](t) = \sum_{i=1}^n (k_i \dot{y}(t) + b_i) H_{ri}[S(y)](t) \quad (3)$$

where  $\mathbf{k} = [k_1, k_2, \dots, k_n]^T$  and  $\mathbf{b} = [b_1, b_2, \dots, b_n]^T$  are the slope and offset coefficients.

### 2.2. A polynomial module

After an experimental trial-and-error process, it can be found that the rate-dependent P–I model is unable to fully describe the overall nonlinear behavior, especially the nonlinearities caused by modeling error and physical structure. There exists one amplitude difference. Considering the fact that the P–I model is purely a phenomenological model, it is reasonable to add some extra modules into the existing P–I model with serial or parallel

structure. Hereby, a module  $G$  is designed with the following polynomial expression:

$$G: \hat{u}_G(t) = g_1 \hat{u} + g_2 \hat{u}^2 + g_3 \hat{u}^3. \quad (4)$$

This polynomial module is designed to deal with such factors including modeling uncertainty, measurement error, and so on. Theoretically, it can be designed in any complex forms. Yet, the more complex it is, the more calculations the identification procedure will need. After sufficient experimental study, a polynomial form is utilized for the module  $G$ , whose effectiveness will be supported by the experimental results presented in Section 4.

After combining the polynomial module with the inverse P–I model in a serial form, an improved direct inverse rate-dependent P–I model can be derived in the following form:

$$\hat{u}_G(t) = G(\mathbf{w}_h^T \cdot \mathbf{H}_r[S(y)](t)). \quad (5)$$

Finally, the uncertain parameters to be identified turn to be  $\mathbf{k}$ ,  $\mathbf{b}$ ,  $\mathbf{c}$  and  $\mathbf{g}$ , where  $\mathbf{g} = [g_1, g_2, g_3]^T$  denotes the polynomial module coefficient vector.

### 3. Practical feedforward control strategy

#### 3.1. Data preprocessing procedure

Based on the analysis of the input signals and the utilized position sensor, we take the following data preprocessing procedure:

- The control input signals for a PTS could be in a variety of forms. In traditional AFM imaging application, a periodic triangular signal is generally applied to its X-axis together with a staircase signal applied to its Y-axis [11]. However, there exist lots of problems in this scanning pattern: oscillations at the turning points will easily lead to system vibration and instability; this pattern is also time costing. Based on this fact, we apply both amplitude varying sinusoidal signals to the X- and Y-axis to achieve better imaging performance without any oscillation at the turning points (see [21,22]). Then, this spiral scanning pattern produces no waste data and it costs less time.
- The PTS output signals generally contain much noise. To deal with this problem, we apply a medium filter to the output data, which may change the signal's phase as well.
- As for parameter estimation, after some trial-and-error experiments, the initial hysteresis loop is abandoned, and the middle part of the data is utilized to conduct identification, so as to achieve more stable results.
- Alignment for data. In our platform, a high-precision capacitive sensor is utilized to measure the micro displacement. Instead of repeatedly setting the output to zero by users, the output data is aligned symmetric around zero through some data translation procedure.

#### 3.2. Identification process

The parameters to be identified through experimental data are the slope coefficient vector  $\mathbf{k}$ , the offset coefficient vector  $\mathbf{b}$ , the saturation operators coefficient vector  $\mathbf{c}$  and the polynomial module coefficient vector  $\mathbf{g}$ . Inspired by the identification method in [6], we separate the identification process into three steps: Step I. identification of the rate-independent parameter  $\mathbf{c}$ ; Step II. identification of the rate-dependent weights  $\mathbf{k}$  and  $\mathbf{b}$ ; and Step III. identification of all the uncertain parameters  $\mathbf{k}$ ,  $\mathbf{b}$ ,  $\mathbf{c}$  and  $\mathbf{g}$ .

- Firstly, we apply an input signal with low frequency to the PTS, and the whole model can be regarded as rate-independent. Then the rate-independent model defined in (1) is utilized to

obtain the estimated parameters  $\mathbf{w}_h$  and  $\mathbf{c}$ . The nonlinear optimization is implemented in the following manner: set the initial value of  $\mathbf{c}$  as  $\mathbf{c} = [c_1, c_2, \dots, c_m]^T = [1, 0, \dots, 0]^T$ ; use linear least-square method to calculate the initial value of  $\mathbf{w}_h$ ; adopt the LM method to estimate the optimized value. The cost function of this nonlinear optimization is set as follows:

$$J(\hat{\mathbf{w}}_h, \hat{\mathbf{c}}, t) = \hat{u}(t) - u(t) = \hat{\mathbf{w}}_h^T \cdot \mathbf{H}_r[\hat{S}(y)](t) - u(t). \quad (6)$$

In this way, the optimized values  $\hat{\mathbf{w}}_h$ ,  $\hat{\mathbf{c}}$  are obtained.

- Secondly, an input signal with a wide bandwidth and high frequency is applied to the PTS, and the rate-dependent model (3) can be adopted. Based on the initial values obtained in (6), the LM method is then adopted to conduct another nonlinear optimization procedure. The cost function of this nonlinear optimization is set as follows:

$$\begin{aligned} J(\hat{\mathbf{k}}, \hat{\mathbf{b}}, \hat{\mathbf{c}}, t) &= \hat{u}(t) - u(t) \\ &= (\hat{\mathbf{k}}\dot{y}(t) + \hat{\mathbf{b}})^T \cdot \mathbf{H}_r[\hat{S}(y)](t) - u(t). \end{aligned} \quad (7)$$

Then, the optimized values  $\hat{\mathbf{k}}$ ,  $\hat{\mathbf{b}}$ ,  $\hat{\mathbf{c}}$  are obtained.

- At last, adopting the modified model (5), the overall nonlinear optimization procedure is in the following way: set the initial value of  $\mathbf{g}$  as  $\mathbf{g} = [1, 0, 0]^T$ ; set the initial value of  $\mathbf{k}$ ,  $\mathbf{b}$ ,  $\mathbf{c}$  as the estimated values  $\hat{\mathbf{k}}$ ,  $\hat{\mathbf{b}}$ ,  $\hat{\mathbf{c}}$  obtained previously; adopt the LM method to estimate the optimized value. The cost function for this nonlinear optimization is set as:

$$J(\hat{\mathbf{k}}, \hat{\mathbf{b}}, \hat{\mathbf{c}}, \hat{\mathbf{g}}, t) = \hat{G}((\hat{\mathbf{k}}\dot{y}(t) + \hat{\mathbf{b}})^T \cdot \mathbf{H}_r[\hat{S}(y)](t)) - u(t). \quad (8)$$

Till this point, all the uncertain parameters have been successfully determined as  $\hat{\mathbf{k}}$ ,  $\hat{\mathbf{b}}$ ,  $\hat{\mathbf{c}}$ ,  $\hat{\mathbf{g}}$ .

#### 3.3. Practical feedforward control law construction and application

Based on the obtained model, a practical feedforward control law, whose scheme is illustrated in Fig. 2, is proposed for a PTS. As can be seen from this figure, a direct inverse rate-dependent P–I model, a saturation operator, and a polynomial module constitute this compact controller, whose output signal is directly exerted on the X or Y-piezo. This practical feedforward controller helps the PTS to achieve high-speed trajectory tracking at different frequencies.

Considering the requirements to enable an AFM to accomplish fast imaging tasks, the constructed feedforward law is then combined with a feedback component (usually, a traditional PID controller) to form a combined control strategy with comparatively simple structure, which stabilizes the PTS around each scanning point within sufficiently short time. The structure of the combined control strategy is shown in Fig. 3, where, the direct inverse P–I controller (PIINV) eliminates predictable error to fasten system response, meanwhile, the traditional PID controller offers real-time signal feedback to deal with modeling error and various noise within the system. This combined control strategy is implemented and then employed in a practical AFM system to develop high-speed imaging mode.<sup>1</sup>

## 4. Experimental results and analysis

All the experiments are conducted on a Benyuan CSPM 4000 AFM system shown in Fig. 4, where the piezoelectric tube scanner

<sup>1</sup> It should be pointed out that the spiral scanning pattern introduced in [21,22], instead of the traditional one, is employed in the high-speed imaging mode to further increase scanning speed.

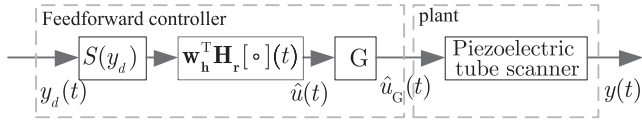


Fig. 2. Feedforward control system.

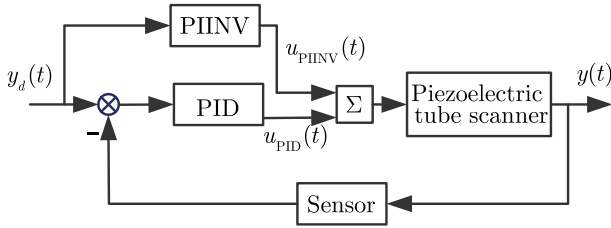


Fig. 3. Feedback and feedforward combined control strategy.

(see Fig. 4(a)) has an approximate displacement range of  $20 \times 20 \times 4 \mu\text{m}$  at the driving voltage range of  $-160 \text{ V}$  to  $+160 \text{ V}$ , and a capacitive microsensors with the sampling period of  $50 \mu\text{s}$  (see Fig. 4(b)) is utilized for displacement measurement. Please note that since the samples are placed on the calibration block, this special structure will lead to the increase of sample scanning scope (much larger than  $20\mu\text{m}$ ).

Firstly, through the data preprocessing procedure, all the measurements are filtered using a medium filter, and aligned to be symmetric around zero automatically. To increase the accuracy of the PTS model, the initial 20,000 data is abandoned, and the middle 40,000 data is adopted for parameters identification and trajectory tracking.

4.1. Parameters identification experiments

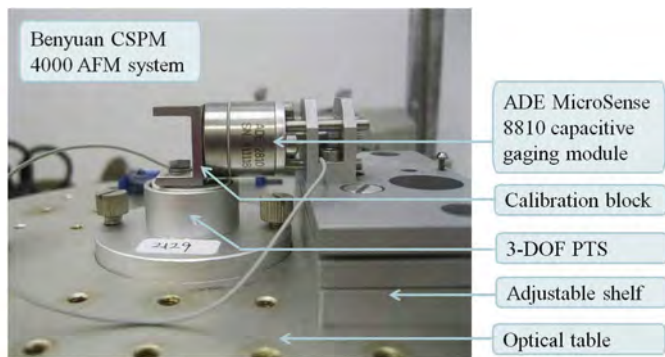
We adopt two sets of input and output experimental data. In the first data set, the control input is selected as a 5 Hz, 150-V p-p amplitude sinusoidal signal to accomplish Step I. for parameters identification. In the second data set, the control input is selected as a superposition of three sinusoidal signals with frequencies of 4 Hz, 23 Hz, and 35 Hz to accomplish Step II. III, explicitly in the following form:

$$u(t) = 50 \sin(8\pi t) + 50 \sin(46\pi t) + 50 \sin(70\pi t) \tag{9}$$

After several trials we finally select  $n = 10$  and  $m = 5$  in (1) and (2). The final identified parameters are shown in Table 1. It should be noted that the parameter identification results are also related with the specific system structure behavior, the selected sampling period, the input/output data amplitude range, and so on.



(a)



(b)

Fig. 4. Experimental setup for a PTS. (a) Piezoelectric tube scanner. (b) Capacitive microsensors setup.

We then utilize another set of data to test the precision of the improved PTS model, with the model verification results shown in Fig. 5, where the actual input coincides very well with the modeled input, convincingly indicating the high precision of the proposed rate-dependent PTS model.

4.2. Trajectory tracking experiments

To verify the modeling and control performance, some trajectory tracking experiments are conducted using the proposed practical feedforward controller. According to the Fourier Transform theory, sinusoidal signals reflect all the period signals essentially in frequency domain. Besides, amplitude varying sinusoidal signals

Table 1  
Parameter identification results.

$i$	$k_i (\times 10^{-4})$	$b_i$	$c_i$	$g_i$
1	1.8278	28.9617	0.9577	3.5203
2	-0.8834	-7.8865	0.0859	-0.0170
3	-0.8037	-1.5569	-0.0055	0.0002
4	-0.2165	-2.4188	-0.0033	
5	0.3884	-0.5172	-0.0001	
6	0.3737	-1.0034		
7	-2.0665	-1.7155		
8	-1.2596	0.4559		
9	6.9434	-1.1909		
10	8.7888	2.7476		

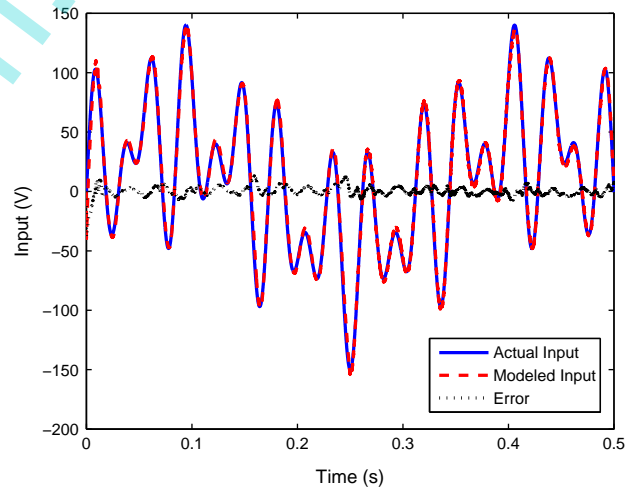


Fig. 5. Model verification results.

can help to achieve better imaging performance in the AFM imaging process [21,22]. For these reasons, we directly apply superposed sinusoidal signals as desired tracking signals.

For these experiments, two desired tracking signals within the identification frequency range are first used to test the tracking performance. The first one is a superposition of three sinusoidal signals with lower frequencies of 7 Hz, 13 Hz, and 19 Hz, explicitly given in the following equation:

$$u(t) = 3.3 \sin(14\pi t) + 3.3 \sin(26\pi t) + 3.3 \sin(38\pi t), \quad (10)$$

while the second one is a superposition of three sinusoidal signals with higher frequencies of 21 Hz, 26 Hz, and 33 Hz:

$$u(t) = 3.3 \sin(42\pi t) + 3.3 \sin(52\pi t) + 3.3 \sin(66\pi t). \quad (11)$$

The tracking performance for these two signals are shown in Figs. 6 and 7, respectively, from which it can be seen that the actual output follows very well with the desired trajectory, with the tracking error mostly less than  $2\mu\text{m}$ .

Besides, to test the robustness of this practical feedforward controller, a superposed tracking signal beyond the identification frequency range is further applied to the system, which is a

superposition of three sinusoidal signals with frequencies of 23 Hz, 34 Hz, and 45 Hz. The tracking performance for this signal is shown in Fig. 8, which is still acceptable with mostly satisfactory tracking precision.

All these tracking experimental results illustrate high-accuracy of the established direct inverse rate-dependent P-I model, and they convincingly demonstrate the satisfactory tracking performance of the designed control strategy.

### 4.3. High-speed AFM imaging experiments

To test the performance of the proposed combined control strategy applied to the AFM high-speed imaging mode, some AFM scanning experiments are conducted on a scanning equidistant stripe grating sample with different control laws. As mentioned above, we adopt the spiral scanning pattern in AFM image scanning instead of the traditional triangular signal pattern, so as to avoid possible oscillations at the turning points and save scanning time. The parameters for the spiral scanning pattern are set as follows:

$$\text{num}_{\text{curves}} = 400, \quad r_{\text{max}} = 160 \cdot k_{\text{factor}} \text{ V}, \quad v = 50,000 \cdot k_{\text{factor}} \text{ V/s},$$

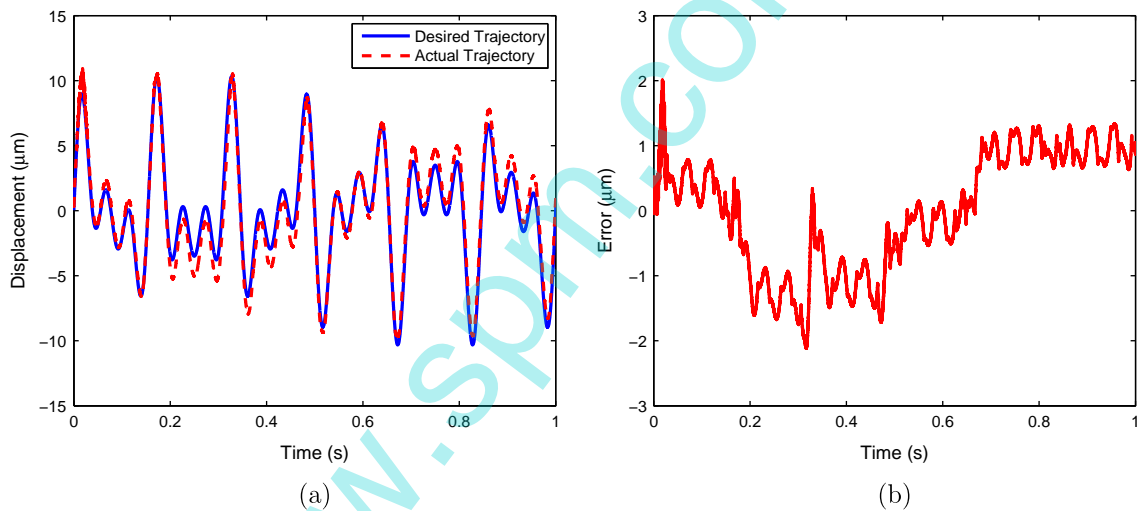


Fig. 6. Trajectory tracking for a lower frequency signal. (a) Desired trajectory and actual trajectory. (b) Tracking error.

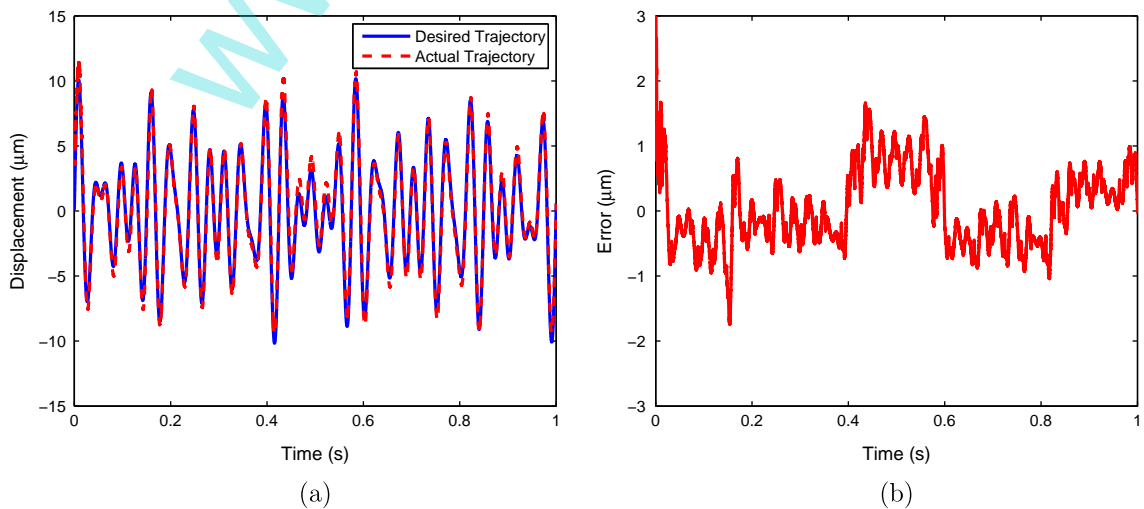


Fig. 7. Trajectory tracking for a higher frequency signal. (a) Desired trajectory and actual trajectory. (b) Tracking error.

$$k_{\text{factor}} = (2.36/160 \times 75/15) \mu\text{m}/\text{V}.$$

where,  $num_{\text{curves}}$  represents the number of times that the spiral curve goes across the line  $y=0$ , which is similar to the image resolution in normal scanning pattern.  $r_{\text{max}}$  is the largest radius

displacement (or voltage when under open-loop control strategy) applied to X/Y-piezo, which is similar to the scanning scope in normal scanning pattern.  $v$  represents the scanning linear velocity which is set constant, and it is closely related to the scanning time.

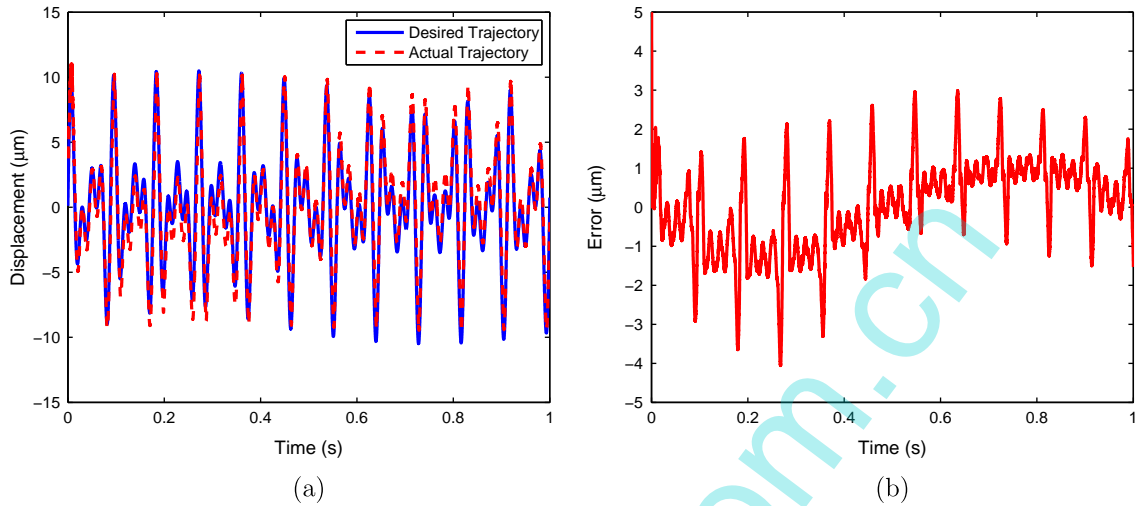


Fig. 8. Trajectory tracking for a frequency overrange signal. (a) Desired trajectory and actual trajectory. (b) Tracking error.

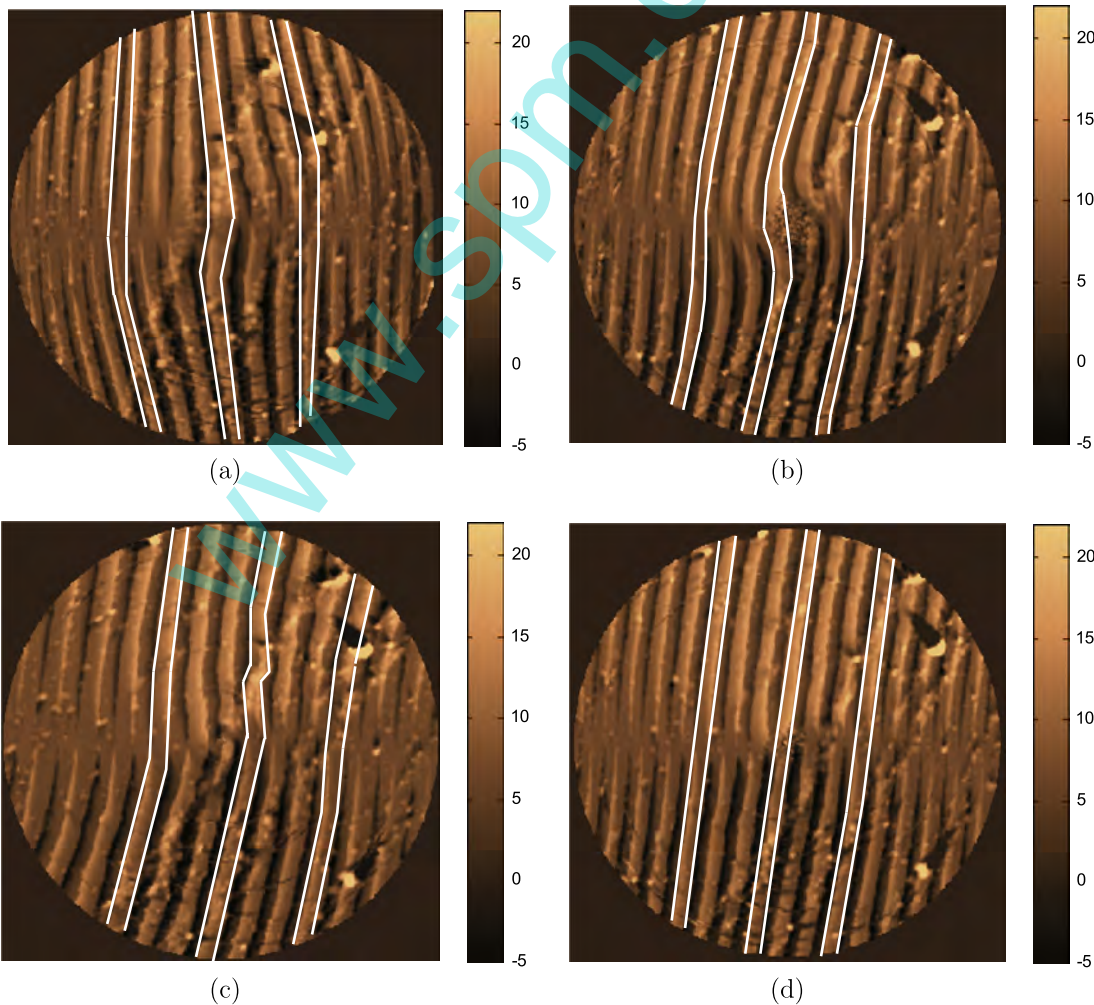


Fig. 9. Image scanning control strategies: (a) open-loop. (b) PID feedback. (c) PIINV feedforward. (d) PID and PIINV combined.

At last,  $k_{\text{factor}}$  denotes the calculating scaling factor, which converts the input voltage into the displacement at the measuring point.

Under the scanning parameters setting, all image scanning process is completed within 23 s, while a similar size image under traditional scanning pattern and control strategy will need more than 40 s at the scanning rate of 10 Hz. It should be noted when better hardware system is adopted, the scanning time for such an image can be further shortened by the proposed control strategy.

Then, we evaluate the tracking performance of high frequency trajectories during image scanning. All the imaging performance under four different control strategies is shown in Fig. 9. Since the lines of the stripe grating sample are straight and equidistant, as long as trajectory tracking performs well, there will exist less image bending, oscillation or distortion (please see [9] for detailed description of these cases). Please note that the six white lines on the images of Fig. 9 are intentionally added to mark out the stripe grating lines, so as to better exhibit imaging performance of different strategies. The detailed analysis for the four control strategies are summarized as follows:

- open-loop control strategy: it clearly shows that due to the hysteresis nonlinearity, the stripe grating lines present bending and unequal horizontal space phenomenon.
- PID feedback control strategy: it shows that some parts display improved performance when compared with the open-loop control strategy, yet it occasionally exhibits even worse performance and twist distortion appears in the image. Wherein, the proportional, integral and derivative gains are respectively chosen as follows:

$$P_G = 0.15, \quad I_G = 0.2, \quad D_G = 0.$$

It can be seen from these results that common feedback controller cannot compensate the nonlinearity effectively.

- PIINV feedforward control strategy: it shows that the direct inverse P–I controller helps to eliminate the hysteresis error to some extent, but it cannot achieve the expected performance. Wherein, the parameters in the feedforward control law,  $\hat{k}, \hat{b}, \hat{c}, \hat{g}$ , are identified through the previous step.
- PID and PIINV combined control strategy: it shows that nearly all the stripes form regular, uniform and straight horizontal space, which fit very well with real sample surface. The adopted parameters of PID controller and PIINV controller are the same as above. The imaging performance clearly shows that the combined control strategy can effectively track high frequency trajectories.

## 5. Conclusion

This paper designs a practical high-speed feedforward tracking control law for a PTS, and then apply it to an AFM to accomplish fast and high-precision image scanning. That is, to achieve satisfactory tracking performance, an improved direct inverse rate-dependent P–I model, together with a polynomial module, is proposed to accurately describe the characteristics of a PTS, which is then utilized to design a feedforward tracking control law to enable the PTS to track a high frequency trajectory. Moreover, based on

the constructed feedforward control law, a practical combined control strategy is proposed and then adopted in an AFM to accomplish high-speed scanning tasks. Finally, sufficient experimental results are provided to demonstrate the satisfactory performance of the proposed model/control strategy. Our future work is planned to focus on further improving the signal tracking accuracy and adopting more advanced control laws to achieve even better imaging performance.

## References

- [1] Mohammadzahari M, Grainger S, Kopaei MK, et al. IMC-based feedforward control of a piezoelectric tube actuator. In: Proceedings of IEEE 8th international conference on Intelligent Sensors, Sensor Networks and Information Processing (ISSNIP); 2013. p. 357–61.
- [2] Aphale S, Fleming AJ, Moheimani SR. High speed nano-scale positioning using a piezoelectric tube actuator with active shunt control. *Micro Nano Lett IET* 2007;2(1):9–12.
- [3] Bhikkaji B, Moheimani SR. Integral resonant control of a piezoelectric tube actuator for fast nanoscale positioning. *IEEE/ASME Trans Mechatron* 2008;13(5):530–7.
- [4] Qi N, Fang Y, Ren X, et al. Varying-gain modeling and advanced DMPC control of an AFM system. *IEEE Trans Nanotechnol* 2015;14(1):82–92.
- [5] Cao Y, Cheng L, Peng JY, Chen XB. An inversion-based model predictive control with an integral-of-error state variable for piezoelectric actuators. *IEEE/ASME Trans Mechatron* 2013;18(3):895–904.
- [6] Qin Y, Tian Y, Zhang D, et al. A novel direct inverse modeling approach for hysteresis compensation of piezoelectric actuator in feedforward applications. *IEEE/ASME Trans Mechatron* 2013;18(3):981–9.
- [7] Binnig G, Quate CF. Atomic force microscope. *Phys Rev Lett* 1986;56(9).
- [8] Devasia S, Eleftheriou E, Reza Moheimani SO. A survey of control issues in nanopositioning. *IEEE Trans Control Syst Technol* 2007;15(5):802–23.
- [9] Leang KK, Zou Q, Devasia S. Feedforward control of piezoactuators in atomic force microscope systems. *IEEE Control Syst Mag* 2009;29(1):70–82.
- [10] Das SK, Pota HR, Petersen IR. Double resonant controller for fast atomic force microscopy. In: Proceedings of 9th Asian Control Conference (ASCC); 2013. p. 1–6.
- [11] Habibullah H, Pota HR, Petersen IR, et al. Tracking of triangular reference signals using LQG controllers for lateral positioning of an AFM scanner stage. *IEEE/ASME Trans Mechatron* 2014;19(4):1105–14.
- [12] Rana MS, Pota HR, Petersen IR. Performance of sinusoidal scanning with MPC in AFM imaging. *IEEE/ASME Trans Mechatron* 2015;20(1):73–83.
- [13] Janaideh MA, Rakheja S, Su CY. An analytical generalized Prandtl–Ishlinskii model inversion for hysteresis compensation in micropositioning control. *IEEE/ASME Trans Mechatron* 2011;16(4):734–44.
- [14] Su C, Liu S, Li Z. Robust adaptive inverse control of a class of nonlinear systems with Prandtl–Ishlinskii hysteresis model. *IEEE Trans Autom Control* 2014;59(8):2170–5.
- [15] Kuhnen K. Modelling, identification and compensation of complex hysteretic nonlinearities – a modified Prandtl–Ishlinskii approach. *Eur J Control* 2003;9(4):407–18.
- [16] Ang WT, Khosla PK, Riviere CN. Feedforward controller with Inverse rate-dependent model for piezoelectric actuators in trajectory tracking applications. *IEEE/ASME Trans Mechatron* 2007;12(2):134–42.
- [17] Su C, Wang Q, Chen X, Rakheja S. Adaptive variable structure control of a class of nonlinear systems with unknown Prandtl–Ishlinskii hysteresis. *IEEE Trans Autom Control* 2005;50(12):2069–74.
- [18] Shan Y, Leang KK. Design and control for high-speed nanopositioning: serial-kinematic nanopositioners and repetitive control for nanofabrication. *IEEE Control Syst Mag* 2013;33(6):86–105.
- [19] Leang KK, Devasia S. Feedback-linearized inverse feedforward for creep, hysteresis, and vibration compensation in AFM piezoactuators. *IEEE Trans Control Syst Technol* 2007;15(5):927–35.
- [20] Guo Z, Tian Y, Liu C, et al. Design and control methodology of a 3-DOF flexure-based mechanism for micro/nano positioning. *Robot Comput Integr Manuf* 2015;32:93–105.
- [21] Rana MS, Pota HR, Petersen IR. Spiral scanning with improved control for faster imaging of AFM. *IEEE Trans Nanotechnol* 2014;13(3):541–50.
- [22] Tian Y, Liu X, Chetwynd D, et al. Nonlinear viscoelastic modelling of stylus probing for surface metrology. *Prec Eng* 2013;37(3):711–20.